Performance Characterization of Supersonic Retropropulsion for Application to High-Mass Mars Entry, Descent, and Landing

Ashley M. Korzun[1] and Robert D. Braun[2]
Georgia Institute of Technology, Atlanta, GA, 30332

Prior high-mass Mars EDL systems studies have neglected aerodynamic-propulsive interactions and performance impacts during the supersonic phase of descent. The goal of this investigation is to accurately evaluate the performance of supersonic retropropulsion with increasing vehicle ballistic coefficient across a range of initiation conditions relevant for future high-mass Mars landed systems. Past experimental work has established supersonic retropropulsion trends in static aerodynamics as a function of retropropulsion configuration, freestream conditions, and thrust. From this experimental database, an aerodynamic-propulsive interactions model is created. EDL system performance results are developed with the potential aerodynamic drag preservation included and excluded during this phase of flight for comparison against prior studies. The results of this investigation demonstrate the significance of aerodynamic drag preservation as a function of retropropulsion initiation conditions, characterize mass optimal trajectories utilizing supersonic retropropulsion, and compare propulsion system requirements with existing propulsion systems and systems under development for future exploration missions.

Nomenclature

A	=	area, m^2
$C_{A,f}$	=	forebody axial force coefficient
$C_{A,total}$	=	total axial force coefficient
C_D	=	aerodynamic drag coefficient
C_T	=	thrust coefficient
g	=	gravitational acceleration, m/s^2
h	=	altitude, m
I_{sp}	=	specific impulse, seconds
L/D	=	lift to drag ratio
m	=	mass, kg
M	=	Mach number
q_∞	=	freestream dynamic pressure, Pa
T	=	thrust, N
t	=	time, seconds
T/W	=	vehicle thrust to weight ratio
β	=	ballistic coefficient, kg/m^2
ΔV	=	velocity increment, m/s
γ	=	relative flight path angle, degrees

[1] Graduate Research Assistant, Daniel Guggenheim School of Aerospace Engineering, Student Member AIAA.
[2] David and Andrew Lewis Associate Professor of Space Technology, Daniel Guggenheim School of Aerospace Engineering, AIAA Fellow.

I. Introduction

TO date, the United States has successfully landed six robotic missions on Mars. Including missions launched by the end of the decade, the largest entry mass sent to Mars will be Mars Science Laboratory (MSL) at ~ 3250 kg.[1] The entry, descent, and landing (EDL) systems for these missions rely heavily on extensions of Viking-heritage technology, namely supersonic Disk-Gap-Band (DGB) parachutes and 70º sphere-cone blunt body aeroshells. Supersonic deceleration has been identified as a critical deficiency in extending these heritage technologies to high mass, high ballistic coefficient systems.[1, 3]

A key parameter used to describe an entry vehicle is the ballistic coefficient, or the ratio of entry mass to hypersonic vehicle drag area, defined in Eq. (1). The six successful Mars landers have all had ballistic coefficients under 100 kg/m^2.[1] One or two orders of magnitude increases in landed mass and aeroshell packaging constraints result in significantly higher ballistic coefficients for the entry vehicles required for human Mars exploration (~ 300 kg/m^2 and higher).[1] For these high ballistic coefficient vehicles, the thin Martian atmosphere and the challenge of extending supersonic DGB parachutes to the required dimensions and deployment conditions combine to severely reduce the timeline available for deceleration and the transition from a hypersonic entry vehicle to a terminal landing configuration. For such systems, it is possible that the surface will be reached while traveling at a supersonic speed.[1] Systems-level studies to assess the required performance of high-mass entry systems recommend the development of alternative supersonic decelerators, a challenge potentially addressed by supersonic retropropulsion (SRP).[1]

$$\beta = \frac{m_{entry}}{C_D A} \tag{1}$$

Supersonic retropropulsion is the initiation of a propulsive deceleration phase while the vehicle is traveling supersonically. Results from wind tunnel experiments in the 1960s and early 1970s show significant preservation of aerodynamic drag during a supersonic retropropulsion phase for peripheral retropropulsion configurations at low to moderate thrust levels.[2] The degree of aerodynamic drag preservation is strongly dependent upon the location of the nozzles on the vehicle forebody and the relative strength of the exhaust flow to the freestream.[5-10] For example, little or no preservation of aerodynamic drag has been experimentally demonstrated for configurations which thrust along the body centerline. The primary parameter used to characterize the static aerodynamics and flowfield stability of the aerodynamic-propulsive interaction is the thrust coefficient (defined in Eq. (2)), with the greatest degree of aerodynamic drag preservation occurring for peripheral retropropulsion configurations with low thrust coefficients. Note that C_T is a force coefficient and is not a direct function of the nozzle geometry.

$$C_T = \frac{T}{q_\infty A} \tag{2}$$

Past experimental work has demonstrated supersonic retropropulsion on a small scale, establishing trends in static aerodynamics as a function of retropropulsion configuration, freestream conditions, and thrust.[2] However, most prior high-mass Mars EDL systems studies[1,3] have neglected aerodynamic-propulsive interactions and the associated performance impacts during the supersonic phase of descent. This investigation addresses the applicability, limitations, and performance implications of supersonic retropropulsion technology in the context of future human and robotic Mars exploration missions. The goal of this study is to characterize the performance of supersonic retropropulsion with increasing vehicle ballistic coefficient across a range of relevant initiation conditions. Results are presented with the potential aerodynamic drag preservation included and excluded during this phase of flight for comparison against prior studies. The results of this investigation demonstrate the significance of aerodynamic drag preservation as a function of retropropulsion initiation conditions, characterize mass optimal trajectories utilizing supersonic retropropulsion, and compare propulsion system requirements with existing systems and systems under development for future exploration missions. A sample robotic scale case is presented for comparison with the human scale cases considered in this study.

II. Approach

In this study, the hypersonic and supersonic phases of a Mars entry trajectory are modeled and simulated. Supersonic retropropulsion is utilized to decelerate the vehicle to the desired terminal state. The analysis is performed as a single-objective optimization problem. Vehicle ballistic coefficients of 200, 400, and 600 kg/m^2 are

considered for the human-scale cases, and an MSL-derived case is considered for comparison with future robotic-scale missions. All cases are constrained by the same initial and final altitude and velocity conditions (those at the atmospheric interface and retropropulsion termination).

A. Methods

In this investigation, the three-dimensional translational equations of motion are integrated from a specified set of initiation conditions (altitude, mass, Mach number, and flight path angle) to Mach 0.9, the subsonic terminal condition used in this study. The Program to Optimize Simulated Trajectories (POST) was used for hypersonic lifting entry phases, and a MATLAB-based simulation was used for SRP phases. A spherical, rotating planet was assumed, as the vehicle is likely to travel significant downrange distances during supersonic descent. Gravity, thrust, and aerodynamic drag forces are modeled over the trajectory, with thrust modeled as constant (no throttling). Mars and its atmosphere were assumed to rotate with constant angular velocity. A hypersonic lifting entry is modeled that transitions to a ballistic supersonic retropropulsion descent. Aerodynamic force coefficients are interpolated between tabulated points as a function of Mach number (hypersonically) and Mach number and thrust coefficient (supersonically). A tabulated atmosphere (-2.5 km to 128 km) based on a nominal Mars Pathfinder entry mission scenario is used for all density, pressure, and temperature values as functions of altitude.

B. Vehicle Configuration and Propulsion Model

The vehicle is assumed to be a 70º sphere-cone with three axially-aligned, bipropellant engines at the periphery of the forebody. Past work by Christian et al.[3] showed that for a blunt entry body, a propulsive configuration with the engines towards the forebody periphery provides more useful volume for payload and propellant tanks than a cluster of engines at the center. An example of a peripheral retropropulsion configuration is given in Fig. 1.

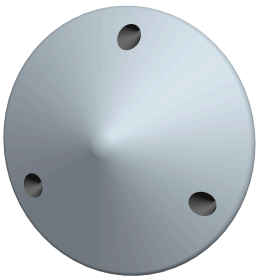

Figure 1. Retropropulsion Configuration.

In the supersonic descent phase, mass is updated as a part of the vehicle state at each time step by the relation given in Eq. (3). The propulsion system was assumed to be LOX/CH_4 with an I_{sp} of 350 seconds. The supersonic descent propellant mass fraction (PMF) is determined by dividing the required propellant mass by the initial vehicle mass. The maximum thrust magnitude is determined from a specified vehicle *T/W*, using the initial vehicle mass and a maximum vehicle *T/W* (Mars) of 3.0.

The engines are scaled with thrust using Eq. (4), a relation developed by Christian et al.[3] through a regression analysis of data for conceptual LOX/CH_4 engines. The engine sizing is used to compare performance requirements of the propulsion systems in this study to existing liquid bipropellant systems.

$$\frac{dm}{dt} = \frac{T}{I_{sp} g_E} \tag{3}$$

$$m_{engine} = 0.00144T + 49.6 \tag{4}$$

C. Aerodynamic-Propulsive Interactions Model

The aerodynamic-propulsive interactions model used during the supersonic retropropulsion phase is based on experimental work by Jarvinen and Adams[5,6] for a peripheral retropropulsion configuration, similar to the one shown in Fig. 1. The experimental data used to construct the model, as well as a comparison between peripheral and central retropropulsion configurations, are given in Fig. 2.

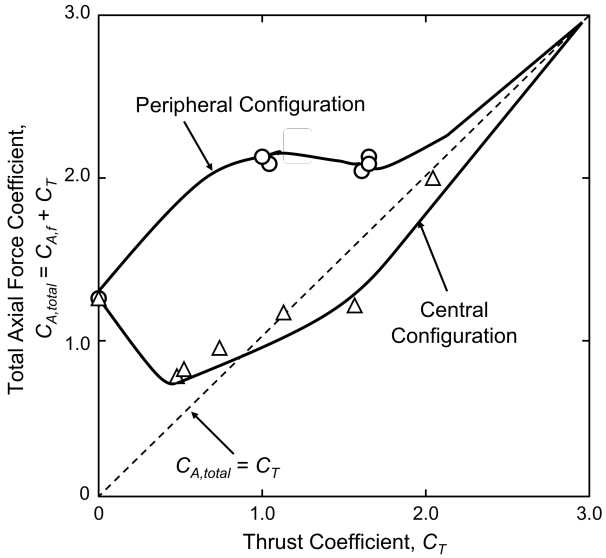

Figure 2. Experimental Data for Total Axial Force Coefficient as a Function of Thrust Coefficient.[5]

For a given vehicle *T/W* and trajectory conditions, the aerodynamic-propulsive interactions model is referenced to determine the total axial force. While the current form of the model does not include variations with Mach number, McGhee[7], with Jarvinen and Adams[5,6] and Keyes and Hefner[10], observed only minor variations in axial force coefficient with C_T across initiation Mach numbers of 2.0 to 6.0. The trajectory conditions must require a deceleration force greater than the aerodynamic drag provided by the blunt body for the model to be active. For thrust coefficients above 3.0, the deceleration force coefficient is equivalent to the thrust coefficient and no aerodynamic adjustment to the thrust coefficient is applied. Figure 3 illustrates the fraction of "no thrust" C_D preserved as a function of C_T for both a peripheral and a central retropropulsion configuration.

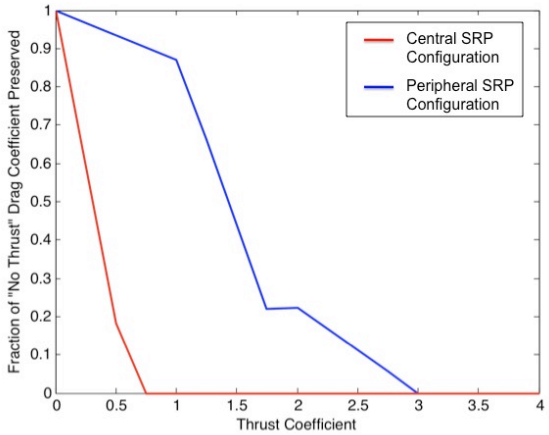

Figure 3. Aerodynamic-Propulsive Interactions Model.

D. Vehicle Mass Model

The following table gives approximate vehicle entry masses corresponding to the hypersonic ballistic coefficients used in this study for 10, 12, and 15 m diameter aeroshells. This entry mass range is consistent with those assumed in NASA Design Reference Architecture 5.0[11] and other studies of future human Mars exploration systems.[2,3,12]

Table 1. Entry Masses (kg) for Various Diameter Aeroshells.

Hypersonic Phase	10 m	12 m	15 m
β = 100 kg/m^2	13305	19160	29937
β = 200 kg/m^2	26611	38320	59875
β = 300 kg/m^2	39916	57479	89812
β = 400 kg/m^2	53222	76639	119749
β = 500 kg/m^2	66527	95799	149686
β = 600 kg/m^2	79833	114959	179623

III. Systems Study Results

This section presents the results of a systems-level performance assessment of supersonic retropropulsion. To initiate this assessment, the supersonic retropropulsion flight segment was modeled. This provided an understanding of the trends and relationships between vehicle ballistic coefficient, initiation conditions (altitude and Mach number), thrust profiles, and supersonic descent propellant mass fraction. With the supersonic performance bounded, the complete entry trajectory performance assessment is completed.

If aerodynamic drag is not a significant factor, the propulsion system will always turn on as late as possible (i.e., at the lowest altitude and lowest velocities permitted by the vehicle *T/W* and other mission constraints) to minimize propellant mass required. This is the case for a gravity turn, where if *T/W* is not constrained, the solution for minimum propellant mass is an infinite thrust magnitude for zero time. In the absence of a aerodynamic-propulsive interaction, constraining *T/W* alters the mass optimal solution to be the maximum allowable thrust magnitude for the minimum amount of time possible to achieve the terminal condition. Because the SRP aerodynamic-propulsive interaction provides the greatest degree of drag preservation at low thrust coefficients (see Fig. 2), the optimal propulsive phase may initiate earlier and decelerate at a reduced thrust level in cases where the drag deceleration is significant. This trade between velocity change required, velocity losses, and available timeline was studied using supersonic trajectories. Descent propellant mass fraction was minimized across a range of vehicle ballistic coefficients (200 kg/m^2 – 600 kg/m^2) and initiation flight path angles (-15º – -75º).

A. Initiation Velocity

Provided there is sufficient thrust available and the drag force is not significant, the retropropulsion phase will begin as late as possible, where the thrusting time is the least. Of the vehicle energy that must be dissipated through retropropulsion and aerodynamic drag, the kinetic energy contribution dominates the potential energy contribution. For example, a 10 t vehicle at 670 m/s (~ Mach 3.0) has a kinetic energy of 2.25 GJ. To have an equivalent potential energy, this vehicle would have be at 60.4 km altitude at the same velocity. This altitude is unrealistically high for ~ Mach 3.0 conditions. As such, the optimal solutions are to initiate at the lowest allowable initiation velocity. The altitude at retropropulsion initiation is then dictated by the vehicle *T/W* such that the terminal conditions (Mach number and altitude) are satisfied. This trend is reflected in Table 2 for β = 400 kg/m^2 and terminal conditions of 5 km altitude and 200 m/s (~ Mach 0.9). Each case starts from 670 m/s and a relative flight path angle of 0º.

Table 2. Initiation Altitude Variation With Vehicle *T/W* (Mars) for β = 400 kg/m^2.

	h_{init} (km)	KE (GJ)	PE (GJ)	PMF
***T/W* = 2.0**	10.02	11.95	1.982	0.137
***T/W* = 3.0**	7.029	11.95	1.391	0.129
***T/W* = 4.0**	6.108	11.95	1.209	0.127
***T/W* = 5.0**	5.700	11.95	1.128	0.125

B. Initiation Flight Path Angle

For the same required velocity change, the required initiation altitude increases as the initiation flight path angle steepens. Table 3 summarizes the required initiation altitude and PMF with increasing flight path angle steepness for a 60 t vehicle and an initiation of 670 m/s (~ Mach 3.0). Achieving the retropropulsion initiation conditions shown in this table is a function of the ability to fly a lifting hypersonic portion of the trajectory.

Table 3. Initiation Altitude Variation With Initiation Flight Path Angle.

	h_{init} (km)	PMF
γ_{init} = -15°	12.61	0.169
γ_{init} = -30°	19.42	0.181
γ_{init} = -45°	25.59	0.191
γ_{init} = -60°	30.62	0.199
γ_{init} = -75°	33.86	0.204

Table 3 demonstrates that PMF improves as the flight path angle shallows (and the resulting initiation altitude decreases as gravity losses are minimized. Figure 4 illustrates this trend for initiation altitudes of 10, 12, and 15 km for a vehicle with a ballistic coefficient of 100 kg/m^2. Each case in Fig. 4 assumed SRP initiation at 670 m/s (~ Mach 3.0) and SRP termination at 200 m/s (~ Mach 0.9).

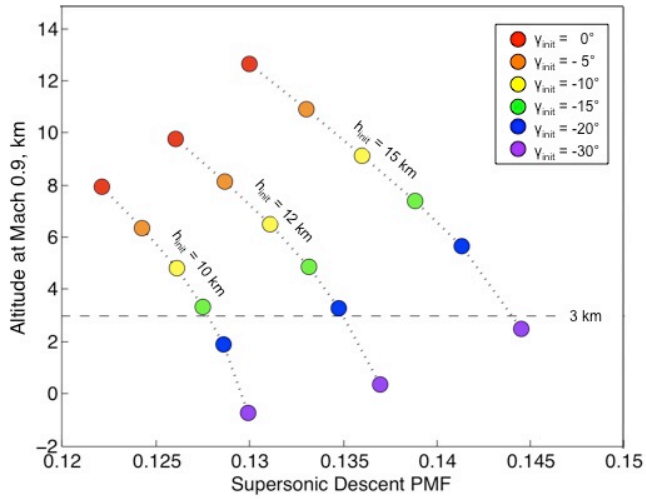

Figure 4. Significance of Initiation Flight Path Angle.

C. Initiation Velocity vs. Drag Preservation

Using Eq. (1) and Eq. (2), the dependency of dynamic pressure on vehicle parameters and thrust coefficient can be determined. This relationship is given in Eq. (5), where C_D is the vehicle hypersonic drag coefficient, and g_0 is the gravitational acceleration at the surface of Mars.

$$q_\infty = \frac{T}{C_T A} = \frac{(T/W)mg_0}{C_T A} = \frac{(T/W)\beta C_D g_0}{C_T} \tag{5}$$

From the relationship given in Eq. (5), the range of initiation conditions for the supersonic retropropulsion phase can be determined in altitude-velocity space. Understanding this range of conditions is important to bound propulsion system required performance and to plan future aerodynamic and aerothermodynamic analysis and test activities. These conditions are constrained by the altitude at which the vehicle reaches Mach 0.9 (with subsequent timeline constraints), Mach number, and dynamic pressure. The dynamic pressure bounds are determined from conditions of nearly full aerodynamic drag preservation (C_T = 1.0) and no aerodynamic drag preservation (C_T = 3.0). Table 4 gives the dynamic pressure bounds for β = 200, 400, and 600 kg/m^2. Figure 5 illustrates these bounds in altitude – velocity space.

Table 4. Dynamic Pressure Bounds.

	$C_T = 1.0$	$C_T = 3.0$
$\beta = 200$ kg/m^2	3.79 kPa	1.26 kPa
$\beta = 400$ kg/m^2	7.56 kPa	2.53 kPa
$\beta = 600$ kg/m^2	11.3 kPa	3.79 kPa

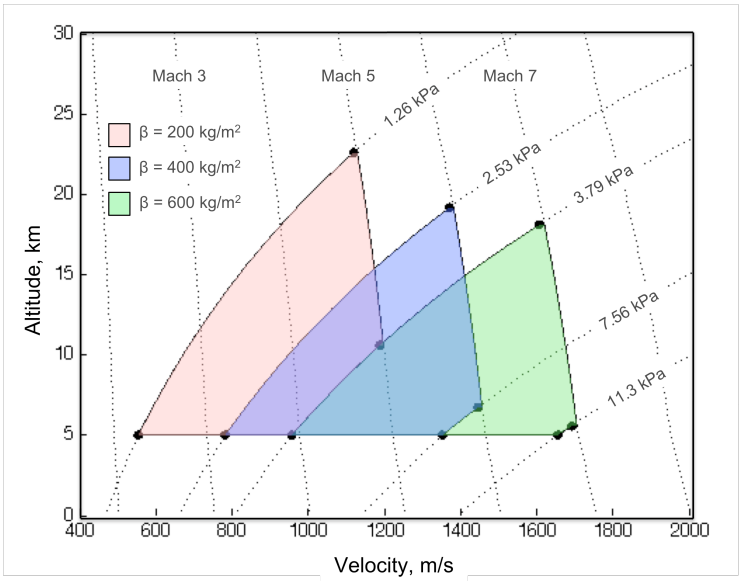

Figure 5. Trajectory Bounds for Aerodynamic Drag Preservation During Retropropulsion Phase.

The four corner points of each shaded region can be used to confirm that lower initiation velocities are preferable, and that for the same initiation velocity, a lower thrust coefficient yields a lower PMF. Note that for the vehicle mass and aerodynamic models used in this investigation, not every corner point condition can be reached ballistically; most require a lifting trajectory.

Figure 4 demonstrated that shallower initiation flight path angles reduce propellant mass. For this reason, the hypersonic lifting trajectories were optimized to determine the bank angle profile and atmospheric entry flight path angle yielding a near-zero flight path angle at the target altitude and velocity conditions (corner points defined in Fig. 5). In the SRP phase, the throttling profile and maximum vehicle *T/W* are determined to minimize the propellant mass fraction required to reach the target terminal conditions of Mach 0.9 at 3 km altitude. The resulting trajectories for ballistic coefficients of 200, 400, and 600 kg/m^2 are shown in Figs. 6 – 8, with a summary of the initiation conditions and required PMF given in Table 5 below.

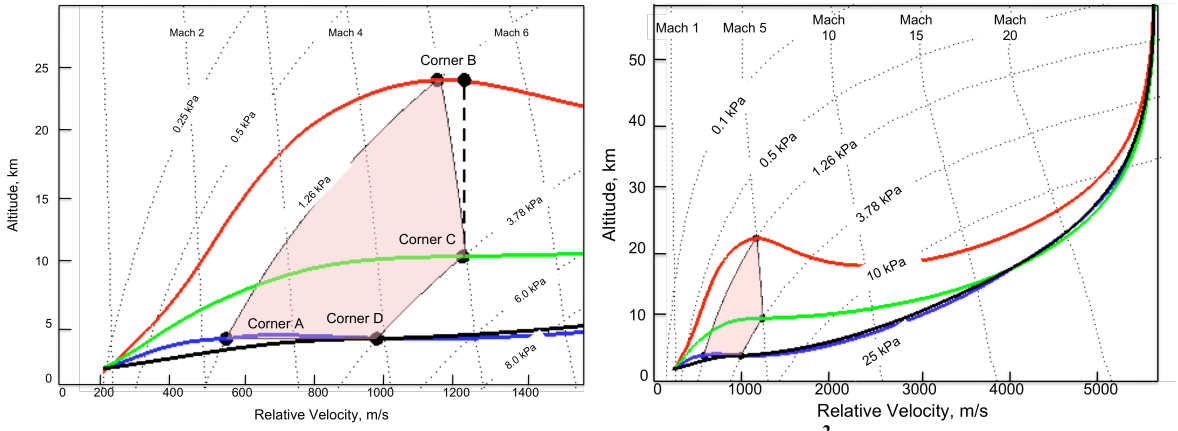

Figure 6. Ballistic Coefficient 200 kg/m^2.

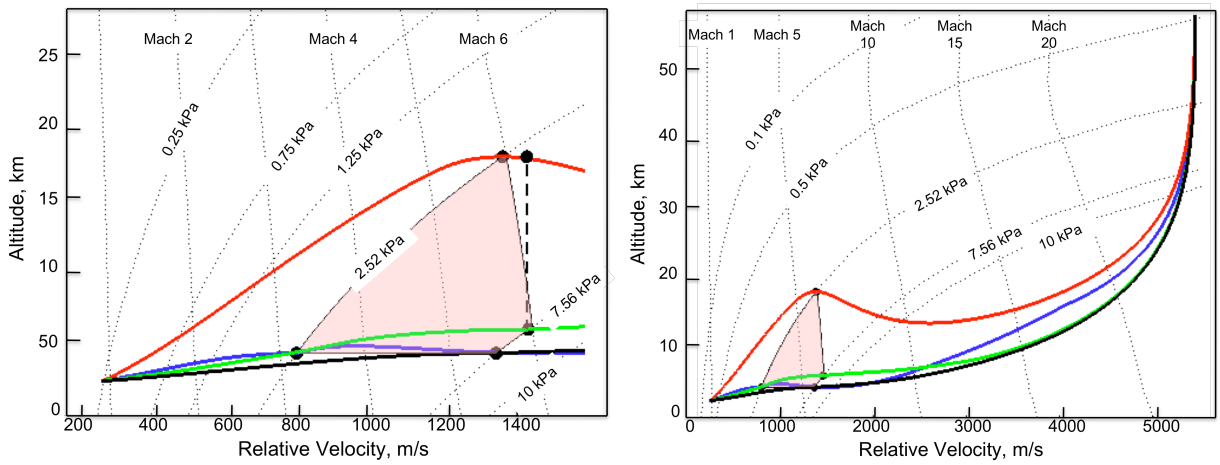

Figure 7. Ballistic Coefficient 400 kg/m^2.

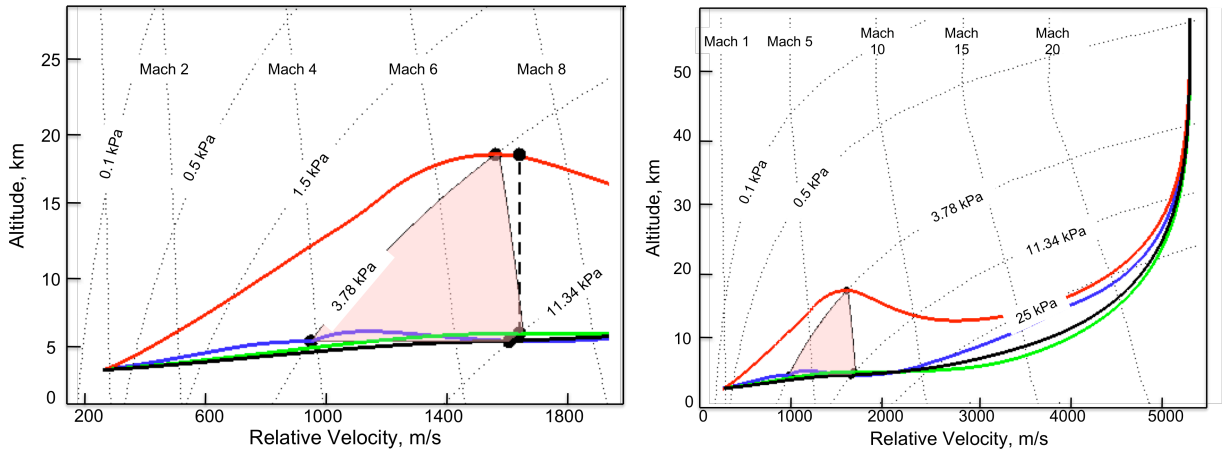

Figure 8. Ballistic Coefficient 600 kg/m^2.

Table 5. SRP Phase Initiation Conditions and PMF Results.

	Altitude (km)	Relative Velocity (m/s)	Relative Flight Path Angle (°)	Max Vehicle *T/W*	Max Thrust (kN)	PMF
β = 200 kg/m^2						
Corner A	5.000	549.76	0.0	3.0	296.8	0.0976
Corner B	22.537	1182.7	0.0	2.0	197.9	0.2667
Corner C	10.576	1182.7	0.0	2.5	247.3	0.2125
Corner D	5.000	952.20	0.0	4.25	420.5	0.1833
β = 400 kg/m^2						
Corner A	5.000	777.47	0.0	4.0	791.5	0.1546
Corner B	19.113	1439.0	0.0	2.5	494.7	0.3086
Corner C	6.7114	1439.0	0.0	5.0	989.4	0.2929
Corner D	5.000	1346.6	0.0	6.0	**1187.3**	0.2784
β = 600 kg/m^2						
Corner A	5.000	952.20	0.0	5.0	**1484.1**	0.1959
Corner B	18.063	1685.4	0.0	3.0	890.5	0.3597
Corner C	5.560	1685.4	0.0	6.5	**1929.3**	0.3466
Corner D	5.000	1649.3	0.0	7.125	**2114.8**	0.3411

Between Corners B and C, which have the same initiation velocity, Corner B has a consistently higher PMF required to reach the target. Corner B corresponds to the $C_T = 3.0$ boundary, and Corner C corresponds to the $C_T = 1.0$ boundary. As expected, for the same required velocity change, lower thrust coefficients enable more aerodynamic drag preservation and yield a lower PMF. While there is also a potential energy effect, since Corner B is always significantly higher in altitude than Corner C, this effect is small in comparison to the difference between C_D preservation for $C_T = 1.0$ (Corner C) and $C_T = 3.0$ (Corner B).

Considering pairings of Corners A and B and Corners C and D, which each have the same C_T constraining their initiation conditions, the corners with the lower initiation velocities have a lower PMF. As discussed in Section III.A, this result is expected as the entry vehicle's kinetic energy scales with the square of the velocity. Removing more energy through retropropulsion requires more propellant. The large difference between Corner A and the other three corners for the $\beta = 200$ kg/m^2 case, as compared to the higher ballistic coefficient cases, is primarily due to the thrust requirements under the constraints of constant thrust and fixed initiation conditions exceeding a C_T of 3.0 (see Section III.E).

Balancing the above two corner comparisons, the impact of initiation velocity is more significant than thrust coefficient at initiation, evidenced by the greater difference in PMF with variation in initiation velocity than with variation in C_T at initiation. In all ballistic coefficient cases examined, Corner A has the lowest PMF, indicating that the optimal initiation conditions are likely to be weighted heavily towards this minimum velocity point (which will occur on the minimum altitude boundary defined by the timeline considerations of the subsequent EDL events). If an upper bound on thrust available is assumed to be 1 MN, at least one corner for each ballistic coefficient in Table 5 can be reached without exceeding this thrust magnitude.

D. Application to Future Robotic Mission

A sample future robotic EDL configuration was derived based on MSL, with an entry mass of 5 t, a 4.5 m diameter 70º sphere-cone aeroshell, and use of the MSL Mars Lander Engines (MLEs). A single MLE was assumed to have a maximum thrust of 3000 N and an I_{sp} of 225 seconds (hydrazine propellant). A single descent stage with 12 MLEs was used for all deceleration not derived from the vehicle's aerodynamic drag. The MSL descent stage has 8 MLEs; use of 12 MLEs increase the vehicle *T/W* (Mars) from 1.23 to 1.94 for a 5 T vehicle.

Two cases were run for comparison: one where no C_D preservation was allowed during SRP and one where a fraction of the "no thrust" C_D was preserved as a function of the thrust magnitude and current dynamic pressure (based on Eq. (5)). An entry flight path angle of -13.65° was assumed and a variable bank angle profile utilized in the hypersonic phase of flight. The conditions at SRP initiation and thrust profile were allowed to vary to minimize the propellant mass required to decelerate to a terminal condition of 2.5 m/s at 50 m above the ground. From these two optimizations, a summary of the differences in required SRP initiation conditions and propellant required is given in Table 6 below.

A third case was run with a vehicle *T/W* (Mars) of 5.0 for comparison; the results are given in Table 6. Increasing the available thrust (by increasing *T/W*) allows the vehicle to initiate SRP later in the trajectory, using the vehicle's aerodynamic drag to reduce the total required ΔV. The increase in *T/W* from 1.94 to 5.0 reduces the required ΔV by 230 m/s as compared to the original case with condition-dependent C_D preservation and by 251 m/s as compared to the original case with no C_D preservation.

Table 6. SRP Performance for 5 t Robotic Cases.

	SRP C_D Preserved	No C_D Preserved	Delayed Initiation
Initiation M_∞	2.85	2.96	1.82
Initiation Altitude	12.95 km	13.67 km	2.76 km
Initiation q_∞	1031.5 Pa	1046.4 Pa	996.2 Pa
C_T at Initiation	2.20	2.16	5.87
***T/W* (Mars)**	1.94	1.94	5.0
m_{prop} Required	1594 kg	1664 kg	1010 kg
PMF	0.319	0.333	0.202

Considering the two cases with an initial *T/W* = 1.94, the 70-kg difference in required propellant mass (a PMF difference of 4.5%) and the difference in initiation conditions show the impact of C_D preservation during the descent phase. For these cases, the maximum thrust available from the 12 MLEs is low enough for C_T to be below 3.0 until the vehicle has decelerated to approximately Mach 2.0. For the *T/W* = 1.94 case with no C_D preservation, this

translates into SRP initiation earlier in the trajectory (higher altitude and Mach number) than for the case with C_D preservation. This is illustrated in Fig. 9 below. Though the thrust profile was not constrained to be constant, the final profiles were of constant thrust in both cases.

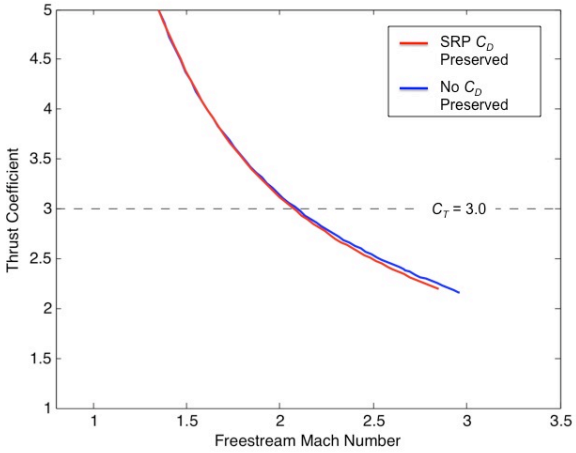

Figure 9. Thrust Coefficient Profile for Robotic Cases (*T/W* = 1.94).

E. Comparison against Prior Human-Scale EDL System Studies

A comparison with a prior human scale Mars EDL study by Christian et al.[3] was completed to illustrate the potential impact of C_D preservation during the SRP phase. The prior study assumed the SRP phase to be modeled by a gravity turn control law with the aerodynamic drag fully preserved and zero lift. The vehicle followed a constant thrust trajectory to a zero-velocity terminal condition 50 m above the surface. The gravity turn control law requires the thrust vector to be maintained in the direction opposite the vehicle's relative velocity vector and the thrust magnitude to be constant. The SRP initiation time was varied to minimize the sum of the propellant and propulsion system masses.

For consistency with the prior study, the vehicle configuration is assumed to be a 15 m diameter Apollo aeroshell with a LOX/CH_4 propulsion system. All trajectories start from orbit (4 km/s) with an inertial entry flight path angle of -14.5°. The trajectories are constrained to a 5g-Earth limit. The design points from Christian et al.[3] and this study are for pure lift-up and lift-down trajectories. For consistency, the design points from this study assume a constant thrust magnitude, constrained to be no larger than 1 MN. The thrust magnitude and initiation conditions are varied to minimize the total propulsion system mass; however, a condition-dependent model for C_D preservation is active during the SRP phase. The aerodynamic-propulsive interactions model for these cases applies the fraction of C_D preserved to the "no thrust" C_D of an Apollo aeroshell instead of a 70º sphere-cone. For comparison against these two SRP modeling approaches, the same cases were simulated assuming no C_D preservation during the gravity turn.

Figure 10 shows the difference between the three C_D preservation assumptions as vehicle ballistic coefficient increases for the L/D = 0.3 cases. The complete results are summarized in Table 7. The data in Table 7 include results from both 10 m and 15 m aeroshell diameters. Table rows with no data are cases that were not able to satisfy the desired terminal conditions without violating the maximum allowable thrust or 5g deceleration constraints.

Figure 10 illustrates that the condition-dependent drag preservation model is better aligned with the assumption of full drag preservation at low vehicle ballistic coefficients and aligned with the assumption of no drag preservation for ballistic coefficients above approximately 300 kg/m^2. Since most human-scale Mars exploration missions that utilize blunt bodies are characterized by large ballistic coefficient vehicles,[3,11] these system studies would be more accurately performed by assuming no aerodynamic drag preservation (or the aerodynamic-propulsive interactions model defined in this investigation) than full drag preservation. In addition, Fig. 10 demonstrates that human-scale Mars exploration missions that utilize slender body aeroshells (generally characterized by lower ballistic coefficients) may be better suited for application of supersonic retropropulsion technology. However, to make definitive statements in this regard, a SRP aerodynamic interactions model for a slender body entry configuration must be developed.

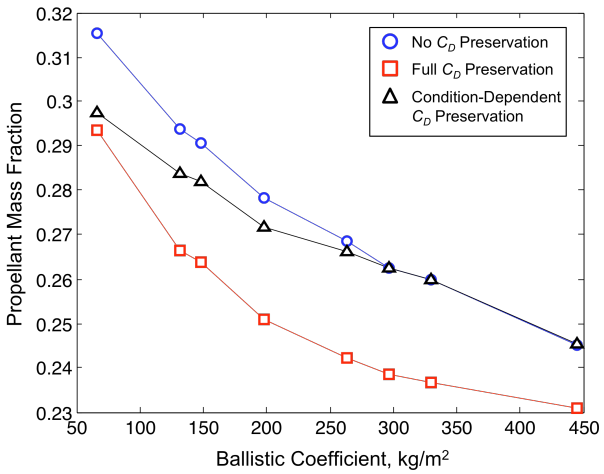

Figure 10. Comparison of C_D Preservation Assumptions with Past Studies.

Table 7. Comparison with Past Study Results

	Initial Mass (kg)	No C_D Preservation	Thrust (kN)	Condition-Dependent C_D Preservation	Thrust (kN)	Full C_D Preservation	Thrust (kN)	% Diff. (Between Cond. and No C_D)	% Diff. (Between Cond. and Full C_D)
L/D = 0.3		PMF		PMF		PMF			
β = 65.94 kg/m^2	18411	0.315	102.8	0.297	85.57	0.294	70.9	5.90	1.27
β = 131.9 kg/m^2	36823	0.294	240.1	0.284	221.1	0.266	176.7	3.49	6.30
β = 148.4 kg/m^2	18411	0.291	121.7	0.282	113.0	0.264	91.1	3.07	6.65
β = 197.8 kg/m^2	55234	0.278	417.7	0.272	396.9	0.251	319.5	2.43	7.93
β = 263.8 kg/m^2	73645	0.268	660.6	0.266	651.5	0.242	523.6	0.83	9.44
β = 296.7 kg/m^2	36823	0.262	358.2	0.262	358.2	0.238	290.0	0.00	9.58
β = 329.7 kg/m^2	92057	0.260	976.0	0.260	976.0	0.237	805.6	0.00	9.33
β = 445.1 kg/m^2	55234	0.245	1026.5	0.245	1026.5	0.231	916.3	0.03	6.03
β = 593.5 kg/m^2	73645	-	-	-	-	-	-	-	-
β = 741.8 kg/m^2	92057	-	-	-	-	-	-	-	-
L/D = 0.5									
β = 65.94 kg/m^2	18411	0.308	108.9	0.283	77.3	0.284	72.4	8.55	0.412
β = 131.9 kg/m^2	36823	0.285	263.9	0.270	233.0	0.253	186.9	5.33	6.48
β = 148.4 kg/m^2	18411	0.281	139.2	-	-	0.248	99.9	-	-
β = 197.8 kg/m^2	55234	0.271	477.3	0.263	447.5	0.240	356.8	2.93	8.90
β = 263.8 kg/m^2	73645	0.260	813.6	0.259	806.0	0.233	643.3	0.31	10.40
β = 296.7 kg/m^2	36823	0.255	454.3	0.256	454.3	0.232	369.4	0.38	9.74
β = 329.7 kg/m^2	92057	0.250	1407.8	0.250	1407.8	0.229	1184.7	0.00	8.67
β = 445.1 kg/m^2	55234	-	-	-	-	-	-	-	-
β = 593.5 kg/m^2	73645	-	-	-	-	-	-	-	-
β = 741.8 kg/m^2	92057	-	-	-	-	-	-	-	-

IV. Concluding Remarks

As vehicle mass increases for missions involving atmospheric entry, supersonic deceleration is challenging the qualifications and capabilities of Viking-heritage EDL technology. At Mars, high entry masses and insufficient atmospheric density often result in unacceptable parachute deployment and operating conditions, requiring the exploration of alternative approaches to supersonic deceleration. Supersonic retropropulsion may be an enabling technology for systems that aim to decelerate large masses in a thin atmosphere, such as at Mars. The relevance of this technology increases with entry mass to the point that it may be required for human Mars exploration.

Across a wide range of ballistic coefficients, efficient supersonic retropropulsion trajectories are characterized by shallow flight path angles at SRP initiation to minimize gravity losses and an initiation velocity that minimizes the required propulsive ΔV. These conditions generally imply SRP initiation at the minimum altitude boundary defined by the timeline considerations of the subsequent EDL events. For the same ΔV, lower thrust coefficients are preferable as they preserve more aerodynamic drag. Overall, however, a lower initiation velocity is preferable over a lower C_T.

For blunt body entry systems and a constant thrust profile, assuming no C_D preservation during SRP is conservative for hypersonic $\beta \leq 300$ kg/m^2. For blunt body entry systems with a hypersonic $\beta \geq 300$ kg/m^2, the thrust coefficient required implies that aerodynamic drag can not be preserved. As such, human-scale Mars exploration blunt body entry systems studies are most accurately performed by assuming no aerodynamic drag preservation (or the aerodynamic-propulsive interactions model defined in this investigation) rather than full drag preservation. In addition, while analysis of a 5 t robotic-scale mission demonstrated a 4.5% PMF advantage to supersonic retropropulsion drag preservation, the *T/W* limitations of the propulsion system assumed in this study constrained SRP initiation to a high altitude, high velocity condition that was shown to be relatively inefficient when in comparison to a higher *T/W* system design.

Past experimental work has demonstrated supersonic retropropulsion on a small scale, establishing trends in static aerodynamics as a function of retropropulsion configuration, freestream conditions, and thrust. The results from this investigation are strongly dependent on the assumed peripheral retropropulsion configuration and limited experimental data. Based on work to date, it is expected that these trends will extend to higher ballistic coefficients as additional SRP configurations are studied and the complexity of the models is increased.

References

[1] Braun, R. D., and Manning, R. M., "Mars Exploration Entry, Descent, and Landing Challenges," *Journal of Spacecraft and Rockets*, Vol. 44, No 2, 2007, pp. 310-323.

[2] Korzun, A. M., Braun, R. D., and Cruz, J. R., "A Survey of Supersonic Retropropulsion Technology for Mars Entry, Descent, and Landing," IEEEAC Paper 1246, March 2008.

[3] Christian, J. A., Wells, G. W., Lafleur, J. M., Verges, A. M., and Braun, R. D., "Extension of Traditional Entry, Descent, and Landing Technologies for Human Mars Exploration," *Journal of Spacecraft and Rockets*, Vol. 45, No. 1, 2008 pp. 130-141.

[4] Vallado, D. A., *Fundamentals of Astrodynamics and Applications*, Microcosm Press, El Segundo, CA, 2001, pp. 908.

[5] Jarvinen, P. O., and Adams, R. H., "The Aerodynamic Characteristics of Large Angled Cones with Retrorockets," NASA Contract No. NAS 7-576, 1970.

[6] Jarvinen, P. O., and Adams, R. H., "The Effects of Retrorockets on the Aerodynamic Characteristics of Conical Aeroshell Planetary Entry Vehicles," AIAA Paper 70-219, 1970.

[7] Romeo, D. J., and Sterrett, J. R., "Exploratory Investigation of the Effect of a Forward-Facing Jet on the Bow Shock of a Blunt Body in a Mach Number 6 Free Stream," NASA TN D-1605, 1963.

[8] McGhee, R. J., "Effects of a Retronozzle Located at the Apex of a 140º Blunt Cone at Mach Numbers of 3.00, 4.50, and 6.00," NASA TN D-6002, 1971.

[9] Peterson, V. L., and McKenzie, R. L., "Effects of Simulated Retrorockets on the Aerodynamic Characteristics of a Body of Revolution at Mach Numbers from 0.25 to 1.90," NASA TN D-1300, 1962.

[10] Keyes, J. W., and Hefner, J. N., "Effect of Forward Facing Jets on Aerodynamic Characteristics of Blunt Configurations at Mach 6," *Journal of Spacecraft and Rockets*, Vol. 4, No. 4, 1967, pp. 533-534.

[11] Drake, B. G., ed., "Human Exploration of Mars: Design Reference Architecture 5.0", NASA-SP-2009-566, 2009.

[12] Marsh, C. L. and Braun, R. D., "Fully-Propulsive Mars Atmospheric Transit Strategies for High-Mass Payload Missions," IEEEAC Paper 1219, March 2009.